A superellipsoid-plane model for simulating foot-ground contact during human gait

D. S. Lopes, R. R. Neptune, J. A. Ambrósio & M. T. Silva

Published online: 01 Sep 2015.

Submit your article to this journal ⬚

View related articles ⬚

View Crossmark data ⬚

Taylor & Francis
Taylor & Francis Group

A superellipsoid-plane model for simulating foot-ground contact during human gait

D. S. Lopes[a,b], R. R. Neptune[b], J. A. Ambrósio[c] and M. T. Silva[c]

[a]INESC-ID Lisboa, Lisboa, Portugal; [b]Department of Mechanical Engineering, The University of Texas at Austin, Austin, TX, USA; [c]IDMEC, Instituto Superior Técnico, Universidade de Lisboa, Lisboa, Portugal

ABSTRACT

Musculoskeletal models and forward dynamics simulations of human movement often include foot–ground interactions, with the foot–ground contact forces often determined using a constitutive model that depends on material properties and contact kinematics. When using soft constraints to model the foot–ground interactions, the kinematics of the minimum distance between the foot and planar ground needs to be computed. Due to their geometric simplicity, a considerable number of studies have used point–plane elements to represent these interacting bodies, but few studies have provided comparisons between point contact elements and other geometrically based analytical solutions. The objective of this work was to develop a more general-purpose superellipsoid–plane contact model that can be used to determine the three-dimensional foot–ground contact forces. As an example application, the model was used in a forward dynamics simulation of human walking. Simulation results and execution times were compared with a point-like viscoelastic contact model. Both models produced realistic ground reaction forces and kinematics with similar computational efficiency. However, solving the equations of motion with the surface contact model was found to be more efficient (~18% faster), and on average numerically ~37% less stiff. The superellipsoid–plane elements are also more versatile than point-like elements in that they allow for volumetric contact during three-dimensional motions (e.g. rotating, rolling, and sliding). In addition, the superellipsoid–plane element is geometrically accurate and easily integrated within multibody simulation code. These advantages make the use of superellipsoid–plane contact models in musculoskeletal simulations an appealing alternative to point-like elements.

1. Introduction

During human movement, the musculoskeletal system is influenced by a number of internal and external contact forces that determine the dynamic response of the system. In order to quantify these forces, contact models are often needed to represent the dynamic interactions between the body segments of interest and the environment. Contact models have been used in applications such as identifying load transfer mechanisms (García-Aznar et al. 2009), muscle contributions to ground reaction forces (Lin et al. 2011; Hamner et al. 2013) and injury mechanisms in car accidents (MADYMO® 2012), and modeling ground contact in walking machines (Koop & Wu 2013) and human–machine interactions (Pasciuto et al. 2014). Musculoskeletal models with ground contact models can even complement experimental analyses that are unable to directly measure ground reaction forces (Lugrís et al. 2013).

Of particular importance for human movement studies is the representation of the foot–ground contact. For studies that do not require complex body segment geometries, a common approach for modeling foot–ground contact is to use kinematic constraints or point-like elements. Kinematic constraints restrict the motion of discrete points along on the sole of the foot (Anderson & Pandy 2003; Lin et al. 2011; Dorn et al. 2012), while point-like elements use a set of discrete viscoelastic elements with Coulomb friction attached to the bottom of each foot segment (Neptune et al. 2000; Peasgood et al. 2007; Mahboobin et al. 2010; Fey et al. 2012). Penalty-based contact force models can have simple representations via point-like elements, or they can have more complex continuous contact force models based on the use of unilateral constraints (Brogliato 2014). However, due to their computational cost and difficulty in handling realistic foot or shoe contact geometries, such unilateral contact models

are often difficult to implement. To a lesser degree, analytical surface contact models have been used to simulate and analyze foot–ground contact. Spheres, ellipsoids, circular cylinders, and planes have been used to model the shoe sole and underlying tissues of the foot (Güler et al. 1998; Kecskeméthy 2011; MADYMO® 2012; Koop & Wu 2013). In particular, ellipsoid contact models have been used in gait analyses to include the double support phase which is an important element in biped walking (Koop & Wu 2013). Other studies have even used the same analytical surfaces to model the articulating surfaces of the knee joint (Wilson & O'Connor 1997; Abdel-Rahman & Hefzy 1998). However, these studies have been limited to specific surfaces and do not explore the potential of more general-purpose shape models such as superellipsoids which are general enough to encompass spherical, ellipsoidal, and cylindrical shapes into a single mathematical expression (Barr 1981). For these methods, a technique to calculate the minimum distances between any convex implicit surfaces has been previously proposed (Lopes et al. 2010), but the mathematical formulation to calculate the closest surface points relies on numerical procedures to solve a non-linear system of equations. Thus, it is a more computationally expensive compared to purely analytical solutions.

Although different geometries have been used to simulate the foot–ground interaction, there are very few studies that have compared the performance of point-like elements with analytical surface models under the same test conditions (Millard et al. 2009; Boos & McPhee 2013). Such a comparison would provide insight into the suitability of analytical surface contact models in human movement analyses. Thus, the objective of this study was to present a general-purpose superellipsoid–plane element model for the simulation of contact interactions during human movement. To illustrate the applicability of the model, we used it in a forward dynamics simulation of walking to represent the foot–ground contact forces. Simulation results and execution times were compared to a similar musculoskeletal model that used point-like elements to model the foot–ground contact to assess whether the more general-purpose surface contact model can provide the same level of efficiency and accuracy as the commonly used point-like contact elements.

2. Methods

2.1. Overview

A three-dimensional musculoskeletal model and forward dynamics simulation of human walking constrained to the sagittal plane were used to compare the contact models. The musculoskeletal model was driven by individual muscle actuators, and dynamic optimization was used to identify the muscle excitations that reproduce group-averaged walking kinematics and ground reaction forces. In order to perform the contact model comparison, two different ground contact geometries were implemented: (1) point-like elements (Neptune et al. 2000) and (2) superellipsoid–plane contact elements. The complete minimum distance formulation is based on the common normal concept (Johnson 1985) and on the angle-center parametric representation of a superellipsoid (Barr 1981). A detailed description of the minimum distance formulism is found in the Appendix. Below we discuss the model components in detail.

2.2. Musculoskeletal model

The forward dynamics simulations were generated using a musculoskeletal model developed with SIMM/Dynamics Pipeline (MusculoGraphics Inc., Santa Rosa, CA) and has previously been described in detail (Neptune et al. 2000; Sasaki et al. 2008; McGowan et al. 2009). The model consisted of rigid segments representing the trunk (a single body representing the pelvis, torso, head, and arms) and two legs (each composed of a thigh, shank, patella, calcaneus, mid-foot, and toes) (Figure 1). The body segments were kinematically constrained using idealized joints with thirteen degrees of freedom in the sagittal plane: two translations and one rotation of the trunk and five flexion–extensions rotations per leg. The hip, ankle, mid-foot, and toe were modeled as frictionless revolute joints, and a planar joint was used at the knee (two translations and flexion–extension rotation, with the translations prescribed as a function of the knee flexion angle (Delp et al. 1990). To model the forces exerted by ligaments and joint structures, passive torques were applied at each joint (Davy & Audu 1987; Anderson & Pandy 1999). The skeletal system was driven by 25 individual Hill-type musculotendon actuators per leg, which were combined into 14 muscle groups based on functional and anatomical classification, with muscles within each group receiving the same excitation pattern (Figure 1). The activation–deactivation dynamics were governed by a first-order differential equation (Winters & Stark 1988; Raasch et al. 1997), and the excitation patterns were parameterized using a bimodal pattern (Hall et al. 2011).

2.3. Continuous contact force model

Both the point-like and ellipsoid–plane contact models utilize a continuous contact force model that considers the minimum distance and relative velocities between two potential contacting geometries, which allows the vertical and horizontal ground reaction force components to be determined. Each contact element permits deformation
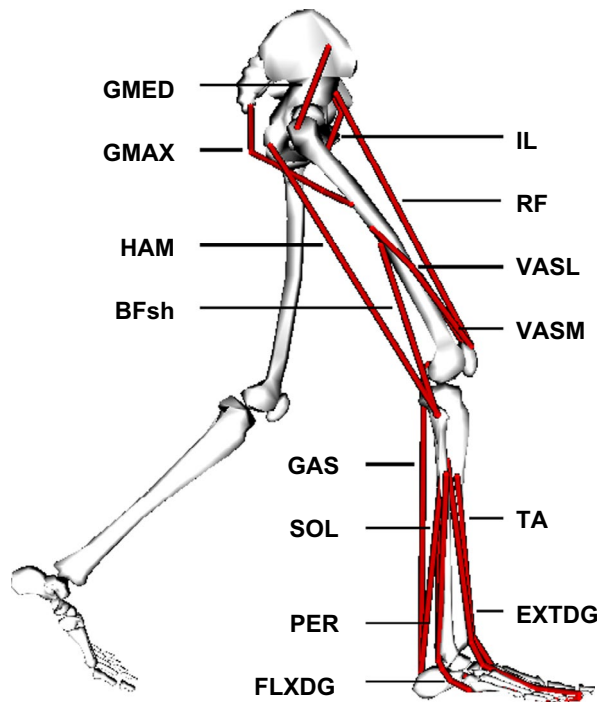
Figure 1. The 3D musculoskeletal model consisted of a trunk segment (a single body representing the pelvis, torso, head, and arms) and two legs (thigh, shank, patella, calcaneus, mid-foot, and toes).

Notes: The model was actuated by 25 Hill-type musculotendon actuators per leg, combined into 14 muscle groups. The muscle groups were defined as GMED (anterior and posterior compartments of the gluteus medius), GMAX (gluteus maximus, adductor magnus), HAM (biceps femoris long head, medial hamstrings), BFsh (biceps femoris short head), IL (psoas, iliacus), RF (rectus femoris), VASL (vastus lateralis, vastus intermedius), VASM (vastus medialis), GAS (medial and lateral gastrocnemius), SOL (soleus, tibialis posterior), TA (tibialis anterior, peroneus tertius), PR (peroneus longus, peroneus brevis), FLXDG (flexor digitorum longus, flexor hallucis longus), and EXTDG (extensor digitorum longus, extensor hallucis longus).

perpendicular to the floor and the normal force model includes the mechanical properties of the shoe sole and underlying soft tissue. The vertical or normal component of the ground reaction force for each element was calculated as:

$$f_{\mathbf{n}}(i) = f_{\mathbf{n}}\big(\delta_{\mathbf{n}}(i), \dot{\delta}_{\mathbf{n}}(i)\big)$$
$$= \max\left(\big\{0.0,\ area(i)\big(c_1\delta_{\mathbf{n}}(i)^{c_2} + c_3\delta_{\mathbf{n}}(i)^{c_4}\dot{\delta}_{\mathbf{I}}\right.$$

(1)

where $f_{\mathbf{n}}(i)$ is the vertical force of element i (units in N); $\delta_{\mathbf{n}}(i)$ and $\dot{\delta}_{\mathbf{n}}(i)$ are the vertical deformation (units in m) and vertical deformation velocity (units in m/s) of element i, respectively; $c_1, …, c_5$ are shoe-specific parameters determined for a soft running shoe; and $area(i)$, the relative element area scaling factor (dimensionless) (Neptune et al. 2000). Shoe-specific parameters and relative areas (i.e. ratios of the contact area during ground contact to the

contact area between foot and impact pendulum) derived from experimentally collected pendulum impact force–deformation curves by Aerts and Clercq 1993.

Each element also prevents the foot from slipping by applying a Coulomb friction force (Cole et al. 1996). The horizontal or tangential contact force component at each element was calculated as:

$$f_{\mathbf{t}}(i) = f_{\mathbf{t}}\big(\dot{\delta}_{\mathbf{t}}(i), f_{\mathbf{n}}(i)\big) = \begin{cases} area(i)c_6\dot{\delta}_{\mathbf{t}}(i), & |f_{\mathbf{t}}(i)| \le c_7 f_{\mathbf{n}}(i) \\ -c_7 f_{\mathbf{t}}(i), & |f_{\mathbf{t}}(i)| < c_7 f_{\mathbf{n}}(i) \end{cases}$$

(2)

where $f_{\mathbf{t}}(i)$ is the horizontal frictional force of element i (units in N); $\dot{\delta}_{\mathbf{t}}(i)$ the horizontal velocity of element i (units in m/s); c_6, viscous damping coefficient for low sliding velocities; and c_7, friction coefficient of the shoe.

2.4. Point-like and ellipsoid–plane contact models

The point-like foot–ground contact model was represented using 31 independent viscoelastic elements with Coulomb friction (Neptune et al. 2000). These contact elements were attached beneath each foot and distributed over the three foot segments in locations that describe the shoe's profile (Figure 2(a)).

The ellipsoid–plane contact model was represented by a set of 6 independent ellipsoid–plane surface pairs, which were rigidly attached to each foot segment and placed within the shoe's boundary (Figure 2(b)). The formulas to calculate the minimum distance between superellipsoidal and planar surfaces are similar as an ellipsoid–plane surface pair, with the difference that ellipsoids are quadric surfaces. These elements are the smoothest and most computationally efficient type of superellipsoids for closest distance computations (see Appendix) and share the same contact force characteristics as their point-like counterpart (i.e. vertical viscoelastic deformation, Coloumb friction, anterior–posterior and vertical contact force model, and shoe parameters), although they differ in how the distance between the foot and ground is calculated. Note that the distribution of either point–plane or ellipsoid–plane elements does not act as a distributed force, rather as a discrete set of concentrated loads where each contact element produces a single force. The calculation of the minimum distance, or amount of deformation, is described in the Appendix and is valid for both ellipsoids and superellipsoids. As for the minimum distance velocity, once the minimum distance points are calculated for each time step, the velocities can be calculated using a forward difference scheme. As for the vertical deformation velocity (Equations (1)–(2)), it is determined by projecting the relative velocity vector over the ground normal vector. Both

(a) **(b)**
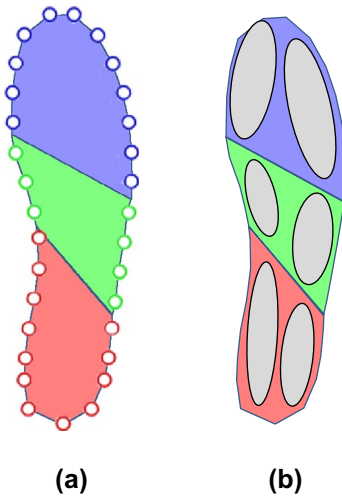
Figure 2. Geometric models of the shod foot in a neutral position with (a) point-like contact elements and (b) ellipsoid–plane contact elements (2D view).
Notes: The foot is considered as a set of three articulated rigid bodies (rear-foot, mid-foot and forefoot) kinematically constrained with revolute joints.

the point-like and surface contact models were developed in C and integrated into SIMM/Dynamics Pipeline via user-defined modules.

2.5. Forward dynamics simulations of walking

The equations of motion for the musculoskeletal model were derived using SD/FAST (Parametric Technology Corp.), and the forward dynamics walking simulation code was produced using Dynamics Pipeline (MusculoGraphics Inc., Santa Rosa, CA). These equations were solved using a variable step integrator (Runge–Kutta–Merson 4th order explicit integration formula with Baumgarte stabilization). Simulations of the entire gait cycle (from left heel-strike to the following left heel-strike) were generated using a simulated annealing optimization algorithm (Goffe et al. 1994), which identified the optimal muscle excitations parameters and initial generalized velocities that minimized the difference between the experimental and group average experimental data (Neptune & Hull 1998). Specifically, the cost function was formulated to minimize the squared differences in joint kinematics and ground reaction forces as:

$$J = \sum_{i} \sum_{m=1}^{17} W_{i,m} \frac{\left(Y_{i,m} - \hat{Y}_{i,m}\right)^2}{SD_{i,m}^2}, \qquad (3)$$

where $w_{i,m}$ is the weighting factor for variable m ($m = 1, \dots, 17$), $Y_{i,m}$ is the experimental measurement of variable m, $\hat{Y}_{i,m}$ is the simulation data corresponding to $Y_{i,m}$ and $SD_{i,m}$ is the standard deviation of experimental variable m

at time step i. The quantities evaluated in (Equation (3)) were the trunk translation and tilt, all joint angles, and the anterior–posterior and vertical ground reaction forces.

2.6. Experimental tracking data

The experimental data were collected from 10 healthy subjects (seven males, three females; 33 ± 12 years) during normal walking (Silverman et al. 2008). All subjects provided informed consent approved by the University of Texas at Austin prior to the study. The data defined the initial conditions for the simulations (positions and orientations of the body segments at left heel-strike) and the experimental tracking quantities in (Equation 3). The data were averaged across trials for each subject and then averaged across subjects to provide the group average kinematic and kinetic data. More details regarding the experimental apparatus, protocol and data processing are provided in (Silverman et al. 2008).

2.7. Contact model performance evaluation

Performance evaluation of the contact models consisted of comparing the execution times over the simulation of a complete gait cycle and accuracy of the experimental data tracking. Numerical integration stiffness was also compared using the temporal evolution of the integration time step sizes (Δt) over the gait cycle. If Δt decreased, then the system equations were considered to have become stiffer. Simulations ran on a PC with an Intel® Core™ i7–3770 CPU @ 3.40 GHz and 8 GB of RAM.

3. Results

Both contact models produced movements that simulated the group average experimental data over the gait cycle, with the sagittal plane joint kinematics and ground reaction forces being near ±2 standard deviations of the experimental data (Figure 3). Root-mean-square errors between experimental and simulated data are provided in Table 1. These results indicate that the ellipsoid–plane surface model is able to attain the same level of tracking accuracy as the point-like contact model. However, there were significant differences in the simulation execution times (Table 2) and integration stiffness of the equations of motion (Figure 4). The average execution time was ~18% faster for the ellipsoid–plane model compared to the point-like model. In spite of the Δt values having the same order of magnitude (10^{-4} s), the numerical resolution of the equations of motion became on average ~37% less stiff when using the ellipsoid–plane contact model.
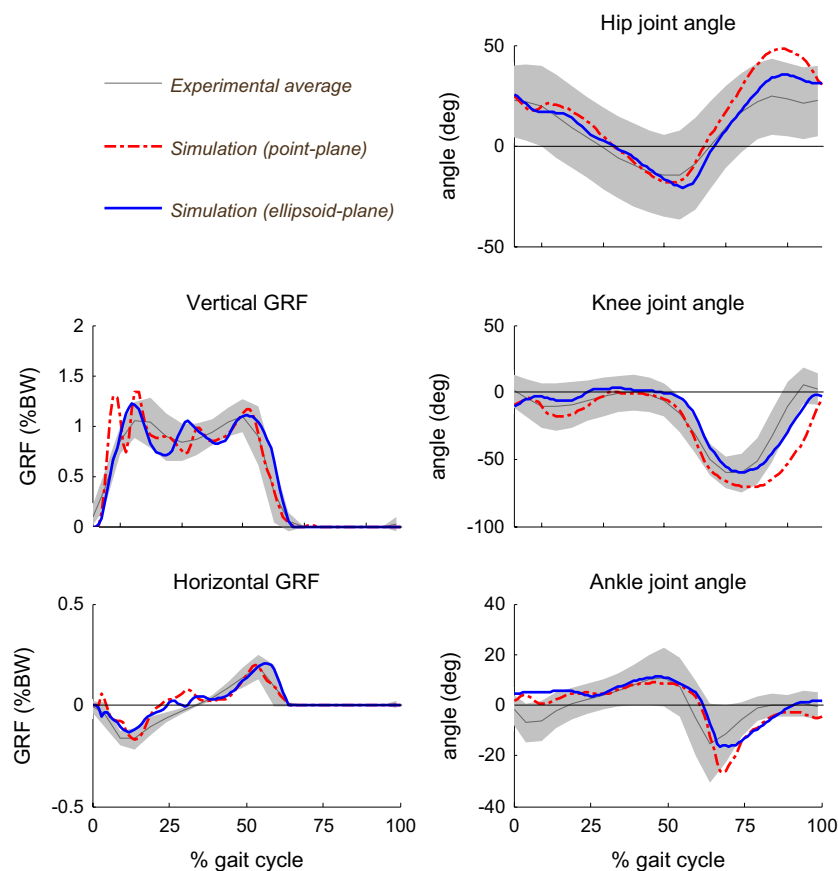
Figure 3. Comparison of the left leg experimental and simulated joint kinematic data and resultant ground reaction forces (normalized to body weight) for the point-like (dash-dot red curve) and ellipsoid–plane (solid blue curve) contact models over the gait cycle. Notes: The shaded regions indicate ±2 standard deviations of the experimental data.

Table 1. RMS errors between left leg experimental and simulated joint kinematic data and resultant ground reaction forces (normalized to body weight) for both contact models over the gait cycle.

| Contact element	Vertical GRF (%BW)	Horizontal GRF (%BW)	Hip joint angle (°)	Knee joint angle (°)	Ankle joint angle (°)
Point-like	0.1260	0.0389	11.2241	16.6217	5.9656
Ellipsoid–plane	0.1198	0.0334	5.6988	8.8686	6.0870

4. Discussion

For musculoskeletal modeling studies that do not require complex body segment geometries, point-like contact elements are the most frequently used to model the foot–ground interactions. However, performance comparisons with more versatile contact elements, such as analytical surfaces, have been few (Millard et al. 2009; Boos & McPhee 2013). The objective of this study was to present a superellipsoid–plane ground contact model and compare it with a point-like counterpart using a common forward dynamics simulation of walking. The results showed they have similar predictive capabilities for the ground reaction forces. However, the superellipsoid–plane contact elements were computationally more efficient (measured in CPU time) than the point-like contact elements and were on average numerically less stiff.

Despite these results supporting the use of superellipsoid elements, there are a few limitations related to the methodology and study comparisons. First, the simulations were two-dimensional. Thus, the potential of superellipsoid–plane elements to model 3D foot motions remains to be explored, in particular foot inversion/eversion. Second, additional movements should be simulated in order to fully explore the limitations of the contact models. Third, further dynamic optimization is needed to improve the tracking results as discrepancies between experimental and simulated data persisted, and the discrepancies were not identical between methods. The dynamic optimization procedure relies on weighting factors which varied between the simulations to obtain the best solutions for the computational comparisons. Since their relative values were determined by trial and error, a more systematic approach may be able to improve the tracking results. Future work should also explore other foot contact model topologies by varying the number,

Table 2. Average execution times and stiffness measures of the performed simulations.

Contact element	Average execution time (s)	Average stiffness measure (s)
Point-like	7.8247	2.4980×10^{-4}
Ellipsoid–plane	6.4205	3.4230×10^{-4}
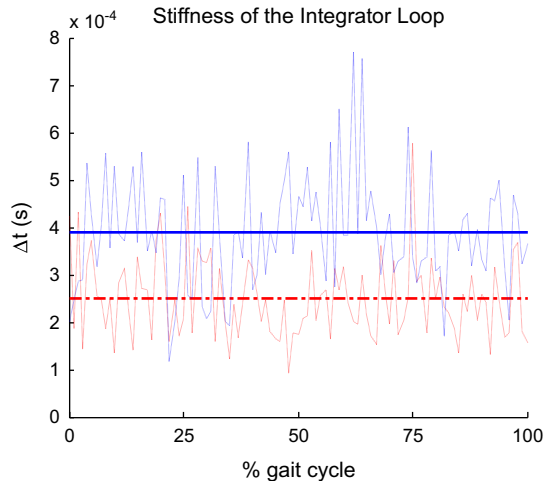
Figure 4. History of integration time steps Δt for the point-like (dashed red plot) and ellipsoid–plane (dashed blue plot) contact models.
Notes: The horizontal lines indicate the average stiffness measures for point-like (dash-dot red) and ellipsoid–plane (solid blue) contact models.

dimensions, orientations, and locations of the superellipsoids to further improve the simulation tracking. Optimization techniques can be used to determine the best foot topology for a given motion. Accordingly, sensitivity studies on how foot–ground contact parameters affect the simulation tracking could then be carried out (Dorn et al. 2012). Fourth, the analytical deduction of the closest points is only applicable to smooth convex surfaces that present an explicit relationship between the surface points and surface normals (Goffe et al. 1994) (refer to Appendix A.3).

Another potential limitation is the limited comparison between contact element layouts. In this study, only a single layout comparison was performed which considered a particular configuration of six ellipsoids placed within the foot sole to an equivalent layout of 31 point-like elements, which were placed at the shoe's profile. Other ellipsoid and point-like layouts should be considered and compared to verify that the same findings (i.e. increased computational efficiency and decreased numerical stiffness) are attained. Such comparisons, where the layouts vary in contact element number and placement, would explore the sensitivity of the results regarding layouts and address, for instance, if a layout with fewer points would lead to different outcomes when compared to a six ellipsoid layout.

Regarding the number of point-like or superellipsoids elements used in the considered layouts (Figure 2), two specific notes must be mentioned. First, regarding the point-like layout, adding additional points increases the number of calculations needed and therefore decreases the computational efficiency. Similarly, decreasing the number of point-like elements (e.g. to 6) increases the stiffness of those elements which also adversely influences the computational efficiency. Previous work has found that an optimal number is ~31 point-like elements (Neptune et al. 2000), which is what is used for the comparison. Second, regarding the ellipsoid layout, it is important to note that the placement of at least two ellipsoids at the heel provides a more stable support during heel ground contact compared to a single heel ellipsoid or sphere (Kecskeméthy 2011; Koop & Wu 2013).

A major challenge in directly comparing the different contact models is finding a geometric contact element that is more computationally efficient than a simple point-like element. Any surface model must provide not only a significant increase in computational efficiency, but also produce comparable simulated data that adequately tracks the experimental joint kinematics and ground reaction forces data. Superellipsoid–plane elements provide such a solution. The gain in computational efficiency and reduced numerical stiffness are an advantage over the point-like elements. The gain in efficiency is due to the usage of a decreased number of contact elements (six ellipsoids vs. 31 points for each foot), since a single surface contains continuous points within the body compared to a set of the independent points. However, one should note that point-like elements provide a discrete spatial resolution, while ellipsoids provide a continuous spatial resolution. A single ellipsoid is capable of representing an infinite set of points. Hence, only a few ellipsoid elements are necessary to represent the foot (e.g. six elements), while a greater number of point-like elements are needed to discretize the foot silhouette (e.g. 31 elements).

Human movement simulations that include continuous contact with a planar surface (e.g. rolling and slipping) would benefit from superellipsoid–plane contact elements since they have several advantages compared to point-like contact elements: (i) geometrically, any point-like contact element can be generalized by a sphere or superellipsoid; (ii) body segment interactions require fewer contact elements when modeled with superellipsoid–plane elements as opposed to point-like elements; (iii) surface overlap is more representative of body deformation than a single point because it can account for contact area and volume, thus allowing volumetric contact; (iv) point models have discrete spatial resolution, while a surface model has a continuous spatial resolution; and (v) surface models allow one to calculate all contact load components (three

forces and three moments) as a function of the kinematic response. In addition, surface contact elements are easily integrated in any multibody dynamics code, which aids the implementation of these models into computational platforms that simulate human movement. Although it is easier to calculate the minimum distance between a point and a plane, the superellipsoid–plane element is equally accurate due to its analytical nature. Points can model complex free-form geometries when gathered as point clouds, which is a common practice in meshfree methods. Superellipsoids are not as versatile; however, they offer a wide variety of shapes ranging from round to square. This broad geometric capability could prove useful when modeling a hard-sole shoe as a set of several cuboid superellipsoids instead of dozens of point-like elements distributed throughout the shoe sole (Mahboobin et al. 2010). In addition, the surface contact model can be used in joint contact mechanics studies. For example, in studies analyzing knee joint contact mechanics, the femoral condyles can be modeled using superellipsoids and the tibial plateau as a plane. These advantages make superellipsoid–plane elements an appealing alternative to point-like contact models for foot–ground dynamics.

Acknowledgments

Disclosure statement

No potential conflict of interest was reported by the authors.

Funding

References

Abdel-Rahman EM, Hefzy MS. 1998. Three-dimensional dynamic behaviour of the human knee joint under impact loading. Med Eng Phys. 20:276–290.

Aerts P, Clercq D. 1993. Deformation characteristics of the heel region of the foot during a simulated heel strike: the effect of varying midsole hardness. J Sports Sci. 11:449–461.

Anderson FC, Pandy MG. 1999. A dynamic optimization solution for vertical jumping in three dimensions. Comput Methods Biomech Biomed Eng. 2:201–231.

Anderson FC, Pandy MG. 2003. Individual muscle contributions to support in normal walking. Gait Posture. 17:159–169.

Barr AH. 1981. Superquadrics and angle-preserving transformations. IEEE Comput Graph Appl. 1:11–23.

Boos M, McPhee J. 2013. Volumetric modeling and experimental validation of normal contact dynamic forces. J Comput Nonlinear Dyn. 8:021006.

Brogliato B. 2014. Kinetic quasi-velocities in unilaterally constrained Lagrangian mechanics with impacts and friction. Multibody Syst Dyn. 32:175–216.

Cole GK, Nigg BM, van den Bogert AJ, Gerritsen KGM. 1996. Lower extremity joint loading during impact in running. Clinical Biomechanics. 11:181–193.

Davy DT, Audu ML. 1987. A dynamic optimization technique for predicting muscle forces in the swing phase of gait. J Biomech. 20:187–201.

Delp SL, Loan JP, Hoy MG, Zajac FE, Topp EL, Rosen JM. 1990. An interactive graphics-based model of the lower extremity to study orthopaedic surgical procedures. IEEE Trans Biomed Eng. 37:757–767.

Dorn TW, Lin Y-C, Pandy MG. 2012. Estimates of muscle function in human gait depend on how foot-ground contact is modelled. Comput Methods Biomech Biomed Eng. 15:657–668.

Fey NP, Klute GK, Neptune RR. 2012. Optimization of prosthetic foot stiffness to reduce metabolic cost and intact knee loading during below-knee amputee walking: a theoretical study. J Biomech Eng. 134:111005.

García-Aznar JM, Bayod J, Rosas A, Larrainzar R, García-Bógalo R, Doblaré M, Llanos LF. 2009. Load transfer mechanism for different metatarsal geometries: a finite element study. J Biomech Eng. 131:021011.

Goffe WL, Ferrier GD, Rogers J. 1994. Global optimization of statistical functions with simulated annealing. J Econom. 60:65–99.

Güler HC, Berme N, Simon SR. 1998. A viscoelastic sphere model for the representation of plantar soft tissue during simulations. J Biomech. 31:847–853.

Hall AL, Peterson CL, Kautz SA, Neptune RR. 2011. Relationships between muscle contributions to walking subtasks and functional walking status in persons with post-stroke hemiparesis. Clin Biomech (Bristol, Avon). 26:509–515.

Hamner SR, Seth A, Steele KM, Delp SL. 2013. A rolling constraint reproduces ground reaction forces and moments in dynamic simulations of walking, running, and crouch gait. J Biomech. 46:1772–1776.

Johnson KL. 1985. Contact mechanics. Cambridge University Press.

Kecskeméthy A. 2011. A novel cylinder-plane foot contact model for human gait motion reproduction. Proceedings of multibody dynamics 2011, ECCOMAS thematic conference; July 4–7, Brussels.

Koop D, Wu CQ. 2013. Passive dynamic biped walking – Part I: development and validation of an advanced model. J Comput Nonlinear Dyn. 8:041007.

Lin Y-C, Kim HJ, Pandy MG. 2011. A computationally efficient method for assessing muscle function during human locomotion. Int J Numer Method Biomed Eng. 27:436–449.

Lopes DS, Silva MT, Ambrósio JA, Flores P. 2010. A mathematical framework for rigid contact detection between quadric and superquadric surfaces. Multibody Syst Dyn. 24:255–280.

Lugrís U, Carlín J, Pàmies-Vilà R, Font-Llagunes JM, Cuadrado J. 2013. Solution methods for the double-support indeterminacy in human gait. Multibody System Dynamics. 30:247–263.

MADYMO®. 2012. Design, simulate and virtual testing. Applications manual, Version 7.4.1, TASS.

Mahboobin A, Cham R, Piazza SJ. 2010. The impact of a systematic reduction in shoe–floor friction on heel contact walking kinematics – a gait simulation approach. J Biomech. 43:1532–1539.

McGowan CP, Kram R, Neptune RR. 2009. Modulation of leg muscle function in response to altered demand for body support and forward propulsion during walking. J Biomech. 42:850–856.

Millard M, McPhee J, Kubica E. 2009. Multi-step forward dynamic gait simulation. In: Bottasso CL, editor. Multibody dynamics: computational methods and applications. Springer; p. 25–43.

Neptune RR, Hull ML. 1998. Evaluation of performance criteria for simulation of submaximal steady-state cycling using a forward dynamic model. J Biomech Eng. 120:334–341.

Neptune RR, Wright IC, van den Bogert AJ. 2000. A method for numerical simulation of single limb ground contact events: application to heel-toe running. Comput Methods Biomech Biomed Eng. 3:321–334.

Nikravesh P. 1988. Computer-aided analysis of mechanical systems. Englewood Cliffs (NJ): Prentice Hall.

Pasciuto I, Ausejo S, Celigüeta JT, Suescun A, Cazón A. 2014. A hybrid dynamic motion prediction method for multibody digital human models based on a motion database and motion knowledge. Multibody Syst Dyn. 32:27–53.

Peasgood M, Kubica E, McPhee J. 2007. Stabilization of a dynamic walking gait simulation. J Comput Nonlinear Dyn. 2:65–72.

Raasch CC, Zajac FE, Ma B, Levine WS. 1997. Muscle coordination of maximum-speed pedaling. J Biomech. 30:595–602.

Sasaki K, Neptune RR, Burnfield JM, Mulroy SJ. 2008. Muscle compensatory mechanisms during able-bodied toe walking. Gait Posture. 27:440–446.

Silverman AK, Fey NP, Portillo A, Walden JG, Bosker G, Neptune RR. 2008. Compensatory mechanisms in below-knee amputee gait in response to increasing steady-state walking speeds. Gait Posture. 28:602–609.

Weisstein EW. 2013. Point-plane distance. From MathWorld – A Wolfram web resource. http://mathworld.wolfram.com/Point-PlaneDistance.html.

Wellmann C, Lillie C, Wriggers P. 2008. A contact detection algorithm for superellipsoids based on the common-normal concept. Eng Comput. 25:432–442.

Wilson DR, O'Connor JJ. 1997. A three-dimensional geometric model of the knee for the study of joint forces in gait. Gait Posture. 5:108–115.

Winters JM, Stark L. 1988. Estimated mechanical properties of synergistic muscles involved in movements of a variety of human joints. J Biomech. 21:1027–1041.

Appendix – Closest point on a superellipsoid to a given plane

A.1. Coordinate transformations

The distance between surface contact elements depends on their rigid body transformations. For each contact surface pair of the foot–ground model, the coordinate systems (Nikravesh 1988)

used that define these spatial configurations relative to the musculoskeletal system are (Figure 5) the global coordinate system XYZ, the rigid bodies coordinate systems $\xi_k \eta_k \zeta_k$, $k \in \{\alpha, \beta\}$, and the surfaces coordinate systems $x_l y_l z_l$, $l \in \{i, j\}$. Position vectors and rotation matrices are represented by $\mathbf{r}$ and $\mathbf{A}$, respectively, while position vectors in the surface reference system are denoted by $\mathbf{s}$. Vector and matrix subscripts indicate the corresponding coordinate systems (e.g. $\mathbf{A}_{O\beta}$ represents the coordinate transformation from the fixed coordinate system of body β to the global coordinate system O). For each surface contact pair, the plane is denoted as surface i and the superellipsoid as surface j.

A.2. Common normal concept

The minimum distance points between a superellipsoid and plane are defined as the surface points that satisfy the common normal conditions (Johnson 1985; Wellmann et al. 2008) and, simultaneously, have the shortest distance between surfaces. The common normal concept consists of the line segment that connects two points, one on each surface, whose normal vectors share a common direction (Figure 6(a)). This concept can be formulated as a set of geometric conditions that assure surface points P and Q have a distance vector, $\mathbf{d}_{PQ}$, which is aligned with the surface normals, $\mathbf{n}_{OP}$ and $\mathbf{n}_{OQ}$ (Figure 6(b)). The collinearity condition between these vectors can be written as two cross product equations relating vectors $\mathbf{d}_{PQ}$, $\mathbf{n}_{OP}$, and $\mathbf{n}_{OQ}$ or equivalently as an orthogonal condition involving vector $\mathbf{d}_{PQ}$, surface tangent vectors $\mathbf{t}_{OP}$ and $\mathbf{t}_{OQ}$, and binormal vectors $\mathbf{b}_{OP}$ and $\mathbf{b}_{OQ}$ (Figure 6(a)).

A.3. Minimum distance points

Contrary to most contact detection procedures that involve superellipsoids, the main characteristic of the applied contact model consists of formulating the minimum distance problem taking as an unknown variable the common normal direction vector (Wellmann et al. 2008) instead of the contact points coordinates (Lopes et al. 2010). Within the superellipsoid family, Barr's surface type (Barr 1981) presents a propitious analytical property for an efficient minimum distance calculation: given a unitary vector, the superellipsoid's radii and exponents along with the surface position and orientation, it is possible to deduce a closed-form expression of the surface point locations that share a common direction with the given vector. Therefore, there is an explicit minimum distance relation between a superellipsoid and a plane since the normal of a plane acts as the given vector.

The considered superellipsoid type has the following implicit representation defined as a dimensionless, real valued scalar function:

$$F_j\left(x_j, y_j, z_j\right) = \left(\left|\frac{x_j}{a_j}\right|^{\frac{2}{\epsilon_1}} + \left|\frac{y_j}{b_j}\right|^{\frac{2}{\epsilon_1}}\right)^{\frac{\epsilon_1}{\epsilon_2}} + \left|\frac{z_j}{c_j}\right|^{\frac{2}{\epsilon_2}}, \ a_j, b_j, c_j \in \mathbb{R}^+ \tag{A.1}$$

where a_j, b_j, and c_j are the radii dimensions along the x_j, y_j, and z_j directions of the local Cartesian coordinates, and ϵ_1 and ϵ_2 are the exponents that affect the roundness (or squareness) of the orthogonal curves that lay on $x_j O y_j$ and $y_j O z_j$, respectively. These exponents, ϵ_k, $k \in \{1, 2\}$, range
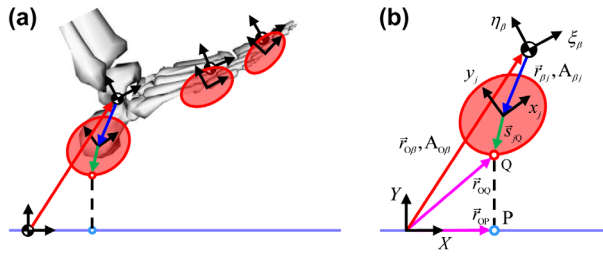
Figure 5. (a) Coordinate systems that describe the spatial configuration of a foot–ground model with superellipsoid–plane contact elements. (b) A zoomed-in view shows the position vectors, rotation matrices, and coordinates systems (global, rigid body, and surface) of a superellipsoidal surface j that represents the heel contact interaction. The model is displayed in the sagittal plane.
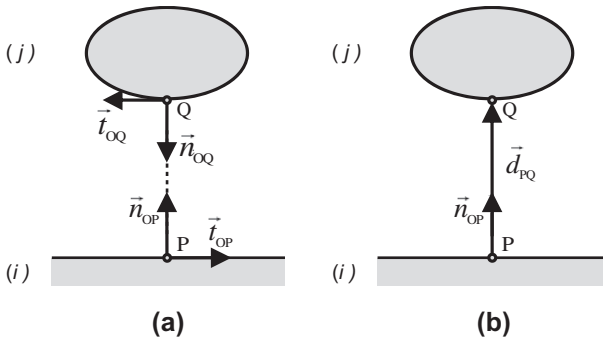
Figure 6. Geometric relationships that define the common normal concept among (a) normal and tangent vectors and (b) the normal and distance vectors.
Notes: Surfaces are represented in 2D, thus, the binormal vectors are not shown. By convention, surface normal vectors point outwards.

between 0 and 2 in order to maintain a strictly convex surface, where $\varepsilon_k \to 0$ leads to a cuboid, $\varepsilon_k = 1$ an ellipsoid, and, $\varepsilon_k = 2$ an octahedron. Note that Fj is written in the canonical form, i.e. surface centered at the origin and the main axes are aligned with the local coordinate system, and is also called as the inside–outside function since its evaluation tells if a point is either inside, outside, or upon the surface. Hence, the equation that defines the geometric loci of a superellipsoid in the canonical form is:

$$F_j\left(x_j, y_j, z_j\right) = 1 \Leftrightarrow \left(\left|\frac{x_j}{a_j}\right|^{\frac{2}{\varepsilon_1}} + \left|\frac{y_j}{b_j}\right|^{\frac{2}{\varepsilon_1}}\right)^{\frac{\varepsilon_1}{\varepsilon_2}} + \left|\frac{z_j}{c_j}\right|^{\frac{2}{\varepsilon_2}} - 1 = 0$$

(A.2)

Furthermore, a superellipsoid can also be represented parametrically using angle-center parameters (Wellmann et al. 2008):

$$\mathbf{s}_{jQ}(\varphi_1, \varphi_2) = \begin{bmatrix} \text{sign}(\cos\varphi_1\cos\varphi_2)a_j|\cos\varphi_1|^{\varepsilon_1}|\cos\varphi_2|^{\varepsilon_2} \\ \text{sign}(\sin\varphi_1\cos\varphi_2)b_j|\sin\varphi_1|^{\varepsilon_1}|\cos\varphi_2|^{\varepsilon_2} \\ \text{sign}(\sin\varphi_2)c_j|\sin\varphi_2|^{\varepsilon_2} \end{bmatrix}, \begin{matrix} -\pi \le \varphi_1 < \pi \\ -\frac{\pi}{2} \le \varphi_2 \le \frac{\pi}{2} \end{matrix}$$

(A.3)

which, by differential calculus, leads to surface normal vectors defined by:

$$\mathbf{n}_{jQ}(\varphi_1, \varphi_2) = \begin{bmatrix} \text{sign}(\cos\varphi_1\cos\varphi_2)a_j^{-1}|\cos\varphi_1|^{2-\varepsilon_1}|\cos\varphi_2|^{2-\varepsilon_2} \\ \text{sign}(\sin\varphi_1\cos\varphi_2)b_j^{-1}|\sin\varphi_1|^{2-\varepsilon_1}|\cos\varphi_2|^{2-\varepsilon_2} \\ \text{sign}(\sin\varphi_2)c_j^{-1}|\sin\varphi_2|^{2-\varepsilon_2} \end{bmatrix}, \begin{matrix} -\pi \le \varphi_1 < \pi \\ -\frac{\pi}{2} \le \varphi_2 \le \frac{\pi}{2} \end{matrix}$$

(A.4)

where φ_1 and φ_2 are the angles that vary along the x_jOy_j and y_jOz_j plane, respectively, and where $\mathbf{n}_{jQ}$ is the vector $\mathbf{n}_{OQ}$ written in the surface coordinate system.

The common normal concept states that the minimum distance points are such that the superellipsoid's surface normal at this point, $\mathbf{n}_{OQ}$, is parallel to the plane's normal, $\mathbf{n}_{OP}$. To express the normal vector of plane i in the local coordinate system of the superellipsoid j, this vector is transformed as:

$$\mathbf{n}_\pi = \left(\mathbf{A}_{O\beta}\mathbf{A}_{\beta j}\right)^{-1}\mathbf{n}_{OP} = \left(\mathbf{A}_{O\beta}\mathbf{A}_{\beta j}\right)^{-1}\mathbf{A}_{O\alpha}\mathbf{A}_{\alpha i}\mathbf{n}_{iP} \quad (A.5)$$

The explicit relationship between the components of $\mathbf{n}_\pi$ and the angular surface parameters, φ_1 and φ_2, comes from the collinearity condition between the plane and superellipsoid normal vectors. This condition can be expressed as the following cross product:

$$\mathbf{n}_\pi \times \mathbf{n}_{jQ} = \mathbf{0} \Leftrightarrow \begin{cases} n_{\pi z}n_{jQy} - n_{\pi y}n_{jQz} = 0 \\ n_{\pi x}n_{jQz} - n_{\pi z}n_{jQx} = 0 \\ n_{\pi y}n_{jQx} - n_{\pi x}n_{jQy} = 0 \end{cases} \quad (A.6)$$

Since $\mathbf{n}_{jQ}$ can be expressed as an angle-center parameterized vector (Equation (A.4)), the explicit expression of the angular surface parameters can be obtained by replacing the components of $\mathbf{n}_{jQ}$ into (Equation (A.5)) and solving in order to find these angular parameters:

$$\varphi_1 = tg^{-1}\left(\frac{\text{sign}\left(n_{\pi y}\right)\left|b_jn_{\pi y}\right|^{\frac{1}{2-\varepsilon_1}}}{\text{sign}\left(n_{\pi x}\right)\left|a_jn_{\pi x}\right|^{\frac{1}{2-\varepsilon_1}}}\right) \quad (A.7)$$

$$\varphi_2 = \begin{cases} tg^{-1}\left(\frac{\text{sign}(n_{\pi z})\left|c_jn_{\pi z}\text{sign}(\cos\varphi_1)\right|\cos\varphi_1|^{2-\varepsilon_1}\right|^{\frac{1}{2-\varepsilon_2}}}{\text{sign}(n_{\pi x})\left|a_jn_{\pi x}\right|^{\frac{1}{2-\varepsilon_2}}}\right), & \left|a_jn_{\pi x}\right| > \left|b_jn_{\pi y}\right| \\ tg^{-1}\left(\frac{\text{sign}(n_{\pi z})\left|c_jn_{\pi z}\text{sign}(\sin\varphi_1)\right|\sin\varphi_1|^{2-\varepsilon_1}\right|^{\frac{1}{2-\varepsilon_2}}}{\text{sign}(n_{\pi y})\left|b_jn_{\pi y}\right|^{\frac{1}{2-\varepsilon_2}}}\right), & \left|a_jn_{\pi x}\right| \le \left|b_jn_{\pi y}\right| \end{cases}$$

(A.8)

Once these angles are calculated, the points on the superellipsoid surface are given by (Equation (A.3)). Note that (Equations (A.7) and (A.8)) present a 0/0 indetermination when $n_{\pi x} = n_{\pi y} = 0$ which only occurs at points $\mathbf{s}_{jQ} = [0, 0, \pm c_j]^T$. It should also be noted that the common normal concept consists of a weak formulation of the minimum distance problem since it states necessary but not sufficient conditions that the two points form a contact pair. In the case of a superellipsoid–plane surface pair,

there are always two possible solutions that verify the common normal conditions (Figure 6). Since the trigonometric relation $\tan(\pi \pm \varphi) = \pm \tan(\varphi)$ holds for any φ and that the tangent term is raised by a multiple of 2 when solving (Equation (A.4)) in order to find φ_1 and φ_2, then there are actually two possible angular values that satisfy the common normal conditions: (φ_1, φ_2) and $(\pi \pm \varphi_1, \pi \pm \varphi_2)$. Therefore, if $\mathbf{s}_{jQ}$ satisfies the common normal conditions then $-\mathbf{s}_{jQ}$ also does. Note that the explicit expressions (Equations (A.7) and (A.8)) are also valid for the 2D case (i.e. superellipse–line) where $\varphi_2 = 0$. After transforming the local position vectors of the superellipsoidal points to global coordinates,

$$\mathbf{r}_{OQ} = \mathbf{r}_{O\beta} + \mathbf{A}_{O\beta}\mathbf{r}_{\beta j} \pm \mathbf{A}_{O\beta}\mathbf{A}_{\beta j}\mathbf{s}_{jQ} \qquad (A.9)$$

the associated points are determined by projecting them to the plane (Weisstein 2013). By evaluating the signed Euclidean distances of these two solutions and by choosing the one with the minimum distance, the contact status is finally determined: (i) If the surfaces intersect at a single point, the minimum distance is zero valued; (ii) for overlapping or fully penetrating surfaces, the distance is considered negative; and (iii) if the surfaces are not contacting, the distance is positive.